



## Synergetic effect of $\text{TiO}_2$ and $\text{Fe}^{3+}$ as co-catalysts for enhanced phenol degradation in pulsed discharge system

Lijuan Duan<sup>a,b</sup>, Nan Jiang<sup>b,c</sup>, Na Lu<sup>b,c,\*</sup>, Kefeng Shang<sup>b,c</sup>, Jie Li<sup>b,c</sup>, Yan Wu<sup>b,c</sup>

<sup>a</sup> School of Environmental Science & Technology, Dalian University of Technology, Dalian 116024, China

<sup>b</sup> Key Laboratory of Industrial Ecology and Environmental Engineering, MOE, Dalian University of Technology, Dalian 116024, China

<sup>c</sup> School of Electrical Engineering, Dalian University of Technology, Dalian 116024, China



### ARTICLE INFO

#### Keywords:

Pulsed discharge plasma  
 $\text{TiO}_2$   
 $\text{Fe}^{3+}$   
 Synergetic effect  
 Phenol decomposition

### ABSTRACT

In this work, the synergetic effect of  $\text{TiO}_2$  and  $\text{Fe}^{3+}$  in pulsed discharge plasma has systematically investigated using phenol as the probe molecule. The dominant effects of  $\text{TiO}_2$  and  $\text{Fe}^{3+}$  dosage were firstly studied, and then phenol degradation was investigated in four parallel experiments including plasma alone, plasma/ $\text{Fe}^{3+}$ , plasma/ $\text{TiO}_2$  and plasma/ $\text{Fe}^{3+}$ / $\text{TiO}_2$ . The experimental results showed that the phenol removal efficiency in plasma/ $\text{Fe}^{3+}$ / $\text{TiO}_2$  system increased by 25% in comparison with plasma alone, which were only 9% and 10% in plasma/ $\text{TiO}_2$  and plasma/ $\text{Fe}^{3+}$  system, indicating a significantly synergistic effect between  $\text{Fe}^{3+}$  and  $\text{TiO}_2$ . To illustrate the synergetic effect of  $\text{TiO}_2$  and  $\text{Fe}^{3+}$  ions, the  $\text{TiO}_2$  structural characterization was analyzed by XPS, UV-vis spectra and XRD, and  $\text{Fe}^{2+}$  and  $\cdot\text{OH}$  concentration was also determined during discharge process. The  $\text{Fe}^{3+}$  ions and excited nitrogen from plasma discharge were doped on  $\text{TiO}_2$  particles, which narrowed the band gap of  $\text{TiO}_2$  from 3.0 eV to 2.0 eV and enlarged the absorption edge at around 600 nm, and therefore enhanced the photocatalytic activity in the visible light. The co-doping of  $\text{Fe}^{3+}$  and nitrogen significantly increased the separation rate of photo-generated electrons and holes and prolonged their lifetime. The photoelectron-transfer pathway was blocked by  $\text{Fe}^{3+}$ , the  $\text{Fe}^{3+}$  ions could be changed to  $\text{Fe}^{2+}$  ions using photoelectron on  $\text{TiO}_2$  surface, inducing Fenton-like reaction for the enhancement of the  $\cdot\text{OH}$  formation rate in the plasma/ $\text{TiO}_2$ / $\text{Fe}^{3+}$  system. The concentration of  $\cdot\text{OH}$  increased from  $14.8 \times 10^{-5}$  mol L<sup>-1</sup> in the plasma/ $\text{TiO}_2$  system to  $20.6 \times 10^{-5}$  mol L<sup>-1</sup> in the plasma/ $\text{TiO}_2$ / $\text{Fe}^{3+}$  system.

### 1. Introduction

Organic compounds in wastewater have become an issue of growing concern in world since the carcinogenic effects of organic compounds have caused severe problems for the human health and environment [1–3]. Advanced oxidation processes (AOPs) have been used with success removal of organic compounds in wastewater over the past few years. Among a wide group of AOPs, the pulsed high-voltage discharge is a promising treatment technology for the effective removal of organic compounds in wastewater, especially high toxic and refractory organic compounds, which are hardly degraded by biological treatment [4–6]. In pulsed discharge plasma system, electrical energy primarily goes into the generation a great amount of high energy electrons, which can excite ambient gases in plasma region to initiate a variety of physical and chemical effects, such as reactive oxidizing species: radicals (H, O, OH) and molecules(O<sub>3</sub>, H<sub>2</sub>O<sub>2</sub>), pyrolysis, ultraviolet light, and shock-wave [7–9]. These chemical and physical effects, in turn, have been proved to efficiently and rapidly remove organic compounds in

wastewater. However, the effects of ultraviolet light radiation and H<sub>2</sub>O<sub>2</sub>, et al. are usually not utilized efficiently in sole plasma discharge, causing low discharge energy utilization efficiency. Recently, the combination of plasma with catalyst, known as plasma-catalyst, has drawn great attention for wastewater treatment.

In early work,  $\text{TiO}_2$  (P-25) powder was applied in pulsed high-voltage discharge systems to utilize ultraviolet radiation from the discharge, exhibiting organic pollutants removal efficiency and energy efficiency were enhanced by addition  $\text{TiO}_2$  into discharge plasma system [10–13]. However, the large band gap of  $\text{TiO}_2$  limits the absorption light wavelength less than 390 nm, resulting in the lower photocatalytic activity of  $\text{TiO}_2$  under visible light. While the pulsed discharge plasma also initiates intensive radiation in visible light region. Luke. et al has reported that an intensive radiation with a wide range of wavelengths (200–1000 nm) from the underwater pulsed corona discharge was observed by the emission spectroscopy [14]. Owing to bare  $\text{TiO}_2$  inherent limitation, the discharge energy of plasma cannot be utilized efficiently in the plasma/ $\text{TiO}_2$  hybrid system.

\* Corresponding author at: Key Laboratory of Industrial Ecology and Environmental Engineering, MOE, Dalian University of Technology, Dalian 116024, China.  
 E-mail address: [luna@dlut.edu.cn](mailto:luna@dlut.edu.cn) (N. Lu).

Therefore, it is an important and challenging issue to enhance  $\text{TiO}_2$  photocatalytic activity under visible light from discharge process, improving the utilization of discharge energy.

One promising route to enhance the photocatalytic performance of  $\text{TiO}_2$  under visible light is to decorate the surface with metal ions. The introduction of metal ions mainly transition metal into  $\text{TiO}_2$  photocatalytic reaction is one of the most simple and efficient way of surface modification [15–17]. Among various transition metal ions,  $\text{Fe}^{3+}$  ion has garnered a great deal of attention due to the remarkable synergic improvement of the  $\text{TiO}_2$  photocatalytic activity in the visible light range. Xing et al. have found that the  $\text{TiO}_2$  doped with  $\text{Fe}^{3+}$  ions shows higher photo-activity under visible light irradiation [18]. It has proved that  $\text{Fe}^{3+}$  ions is an effective doping element on  $\text{TiO}_2$  due to its half-filled electronic configuration, and  $\text{Fe}^{3+}$  implanted  $\text{TiO}_2$  not only favors photoelectrons and holes separation but also narrows the band gap of  $\text{TiO}_2$  [19–21]. More importantly, the reduction of  $\text{Fe}^{3+}$  to  $\text{Fe}^{2+}$  ions by photo-induced electrons on  $\text{TiO}_2$  surface facilitates plasma discharge inducing Fenton-like reactions and thus improves organic pollutants degradation [22]. It is of great value to develop an efficient hybrid process involving  $\text{Fe}^{3+}$  and  $\text{TiO}_2$  photocatalytic oxidation for organic compounds in pulsed discharge plasma. So far, to the best of our knowledge, few researches are published on  $\text{TiO}_2$  and  $\text{Fe}^{3+}$  ions as co-catalyst for degradation of organic compounds in pulsed discharge plasma system.

The aim of this work is to study the synergistic effect of  $\text{TiO}_2$  and  $\text{Fe}^{3+}$  in the pulsed discharge system. Phenol was used as probe molecules to characterize the efficiency of  $\text{TiO}_2$  and  $\text{Fe}^{3+}$  ions. The enhancement of phenol removal efficiency was investigated in four parallel experiments including plasma alone, plasma/ $\text{Fe}^{3+}$ , plasma/ $\text{TiO}_2$  and plasma/ $\text{Fe}^{3+}$ / $\text{TiO}_2$ . Possible mechanisms of such synergistic effect were discussed by analyzing the  $\text{TiO}_2$  structural characterization and were determined the concentration of  $\text{Fe}^{2+}$  and  $\cdot\text{OH}$ . Moreover, the concentration of benzoquinone and hydroquinone was measured to illustrate how co-catalyst improves the efficiency of phenol decomposition by inducing Fenton-like reaction.

## 2. Experimental section

### 2.1. Chemicals

$\text{TiO}_2$  power (Degussa P-25, Germany) has a surface area  $50 \text{ m}^2 \text{ g}^{-1}$  and contains anatase and rutile phases in a ratio of about 3:1. The organic pollutant phenol is analytic grade.

### 2.2. Equipment and procedures

Fig. 1 showed the schematic of experimental set-up. The experimental system consisted of a pulsed high-voltage power supply, a reactor vessel. The needle-plate geometry was used as the electrode system of reactor, which was consisted of the positive needle electrode and ground plate electrode. The positive electrode was five hollow stainless steel needles (4.0 mm in length and 1.0 mm at diameter) and the ground electrode was a stainless steel plate (60 mm diameter). The gas chamber locating at the bottom of reactor was connected with stainless steel needles to bubble air into solution. The electrode distance was adjusted to 10 mm by moving the ground plate electrode. The pulsed high voltage of 20 kV with the pulse frequency of 50 Hz and power input of 9 W was applied on discharge point electrode.

In each batch experiment, 100 mL phenol solution was treated, and the initial concentration of phenol was  $100 \text{ mg L}^{-1}$ . Prior to discharge treatment, air bubbled continuously into the reactor with a flow rate of  $0.05 \text{ m}^3 \text{ h}^{-1}$ . The electrolytic conductivity of experimental solutions was  $100 \mu\text{S cm}^{-1}$ . The suspension of  $\text{TiO}_2$  and phenol solution was stirred for 20 min to establish adsorption-desorption equilibrium prior into the reactor vessel.

All experimental were conducted in duplicates.

### 2.3. Analysis method

The phenol concentrations and its main intermediates (hydroquinone, catechol and benzoquinone) were measured by the HPLC system Shimadu LC-10Avp, equipped with a MS-2 C18 column ( $\varnothing 4.6 \text{ mm} \times 250 \text{ mm}$ ) and a UV detector set at 277 nm. The mobile phase was prepared by the deionized water and chromatographically pure methanol with a flow rate of  $0.8 \text{ mL min}^{-1}$ , and the volumetric ratio between the deionized water and methanol was 70:30 (v/v).

The phenol removal efficiency ( $\eta$ ) is defined as follows,

$$\eta = \frac{C_0 - C_t}{C_0} \times 100\% \quad (1)$$

Where  $C_0$  was the phenol concentration of untreated solution, and  $C_t$  was the concentration of phenol at discharge treatment time  $t$ , respectively.

The method of  $\cdot\text{OH}$  determination relied upon the use of a selective trapping reagent salicylate [23,24]. The resulting two dihydroxylated products 2, 3-DHB and 2, 5-DHB were determined using HPLC system (Shimadu LC-10Avp). The mobile phase consisted of  $0.03 \text{ mol L}^{-1}$  citric acid,  $0.3 \text{ mol L}^{-1}$  glacial acetic acid, methanol (30%, v/v) and acetonitrile (30%, v/v). Elution was performed at a flow rate of

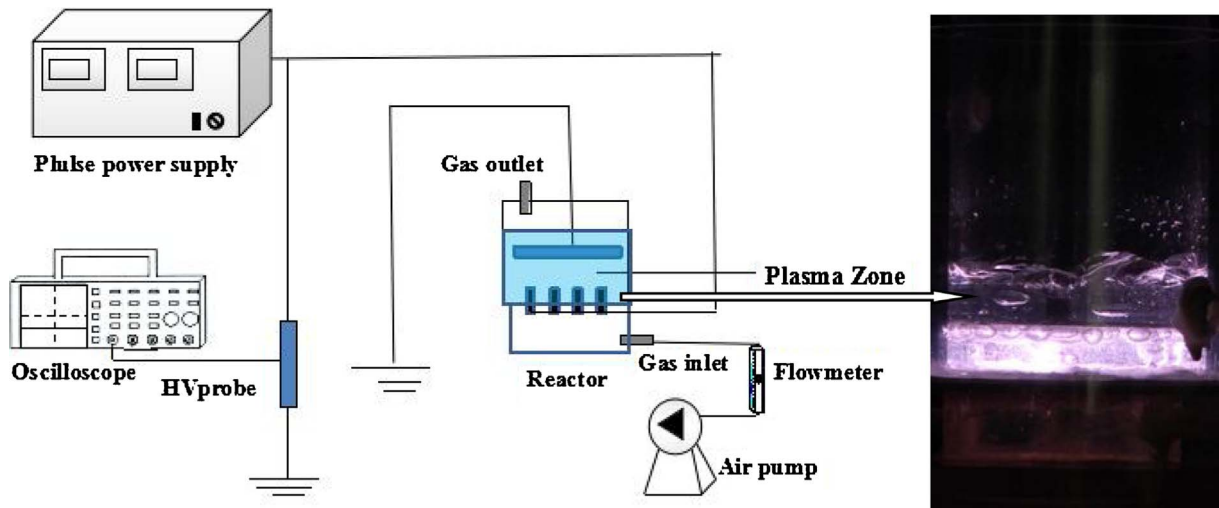


Fig. 1. Schematic diagram of the experimental set-up.

0.8 mL min<sup>-1</sup>.

The concentration of ferrous ions is done by measuring absorbance at a wavelength of 510 nm after colour development by 1, 10-phenanthroline method, and total iron ion was measured by an inductively coupled plasma-atomic emission spectroscopy (ICP-Optima 2000DV).

#### 2.4. *TiO<sub>2</sub>* structural characterization methods

A quantity of 0.02 g TiO<sub>2</sub> powder was introduced into 100 mL aqueous solution under different experimental system. After filtration from different experimental solution, the residue TiO<sub>2</sub> powder was washed three times using distilled water, and then dried at 60 °C for 12 h in stove. Bare TiO<sub>2</sub> power was treated in a similar method and used as a reference.

X-ray photoelectron spectra were recorded on a Jobin Yvon HR800 spectrometer employing a monochromatic Al source. The laser spot size was ~ 1 μm. The shift of binding energy was corrected using the C 1 s peak at 284.6 eV as the reference for calibration. The spectra of Fe2p and N1 s have undergone Shirley background removal and were fit using Voigt functions. X-ray diffraction patterns of all samples were measured by Rigaku D/MAX 2400 diffractometer in the range of 20–80° (2θ), using Cu Kα radiation. UV-vis diffuse reflectance spectroscopy of the TiO<sub>2</sub> samples were measured by Scan UV-vis spectrophotometer (UV-550), using BaSO<sub>4</sub> as reflectance sample.

#### 2.5. Photo-electrochemical measurement

Photocurrents were measured by an electrochemical analyzer (CHI instruments 660E), using the prepared sample film as the working electrode. A 500 W Xe-lamp was used as a light source to irradiate the different working electrode from the back side. A 1.0 M Na<sub>2</sub>SO<sub>4</sub> solution was used as the electrolyte. The working electrodes were prepared by coating different discharge solution onto the indium-tin oxide glass, and then were dried at 100 °C for 1 h.

### 3. Results and discussion

#### 3.1. The synergistic effect of TiO<sub>2</sub> and Fe<sup>3+</sup> on phenol degradation in pulsed discharge plasma

The effects of TiO<sub>2</sub> and Fe<sup>3+</sup> ions dosage on phenol degradation were firstly studied and displayed in Fig. 2(a-b). From Fig. 2(a), the highest removal efficiency of phenol was obtained with the 0.2 g L<sup>-1</sup> TiO<sub>2</sub> dosage. When TiO<sub>2</sub> dosage was lower than 0.2 g L<sup>-1</sup>, the removal efficiency of phenol increased with the enhancement of the TiO<sub>2</sub> dosage. At the same time, when the dosage of TiO<sub>2</sub> was higher than 0.2 g L<sup>-1</sup>, the phenol degradation was a little bit lower than that in sole discharge plasma system. The result could be attributed to the fact that the concentration of photo-generated electron-hole pairs and ·OH became abundant with the increasing TiO<sub>2</sub> dosage, leading to high photocatalytic efficiency. However, when TiO<sub>2</sub> dosage was higher than the optimal concentration, the properties of the TiO<sub>2</sub> suspension influenced the initiation and propagation of the discharge in the liquid phase [25,26]. Therefore, 0.2 g L<sup>-1</sup> TiO<sub>2</sub> dosage was used in the following experiments. As shown in Fig. 2(b), phenol degradation increased firstly and then decreased with enhancement of Fe<sup>3+</sup> concentration, and the optimal concentration of Fe<sup>3+</sup> in the pulsed discharge plasma TiO<sub>2</sub> was 10 mg L<sup>-1</sup>. As discussed in section 3.2, the results indicated that Fe<sup>3+</sup> ions were successfully doped on TiO<sub>2</sub> particles, and the Fe dopant amount could significantly affect photocatalytic activity of Fe-doped TiO<sub>2</sub> because the Fe<sup>3+</sup> could serve not only as electrons and holes trap but also as a recombination center [27,28]. As an optimal concentration of Fe<sup>3+</sup> ions doping on TiO<sub>2</sub> could effectively increase the separation rate of electron-hole pairs, leading to high photocatalytic activity. While the amount of Fe<sup>3+</sup> dopant was higher than the optimal concentration, Fe<sup>3+</sup> dopant became the recombination centers, resulting in

low photocatalytic activity. Therefore, the optimal doping concentration of Fe<sup>3+</sup> ions was 10 mg L<sup>-1</sup> in this study.

To investigate the synergistic effect between Fe<sup>3+</sup> and TiO<sub>2</sub> photocatalytic oxidation, four parallel experiments including plasma, plasma/Fe<sup>3+</sup>, plasma/TiO<sub>2</sub> and plasma/Fe<sup>3+</sup>/TiO<sub>2</sub>, were performed and presented in Fig. 2(c-d). It can be seen that the removal efficiency of phenol was significantly increased in the presence of Fe<sup>3+</sup> and TiO<sub>2</sub> in pulsed discharge system. Fig. 2(c) showed that the phenol removal efficiency was enhanced with the addition of TiO<sub>2</sub> catalyst or Fe<sup>3+</sup> ions compared with plasma alone. In the presence of TiO<sub>2</sub>, the production of photoelectrons-holes pairs and the reactive oxidizing species mainly ·OH and superoxide radicals could promote phenol removal. In the case of Fe<sup>3+</sup> catalyst, Fe<sup>3+</sup> was converted to Fe<sup>2+</sup> through reactions with quinone intermediates, and then Fe<sup>2+</sup> ions induced Fenton reaction to generate more amounts of ·OH, hence phenol removal efficiency was improved. As shown in Fig. 2(d), the phenol removal efficiency in plasma/Fe<sup>3+</sup>/TiO<sub>2</sub> was increased by 25% in comparison with plasma alone, which only increased by 9% and 10% in plasma/TiO<sub>2</sub> and plasma/Fe<sup>3+</sup> system, respectively. Similar results have been reported previously, the introduction of TiO<sub>2</sub> or Fe<sup>3+</sup> into pulsed discharge plasma system could increase phenol removal efficiency, and the promotion removal efficiency was typically range from 9% to 13% [10,13,25]. Therefore, the TiO<sub>2</sub> and Fe<sup>3+</sup> catalyst could be effectively activated in present pulsed plasma discharge system. These results indicated that the individual Fe<sup>3+</sup> and TiO<sub>2</sub> induced reaction didn't simply add up but there indeed existed an obvious synergy between Fe<sup>3+</sup> and TiO<sub>2</sub> in pulsed discharge system. There may be two reasons responsible for this synergistic effect. One probable reason is that Fe<sup>3+</sup> ions can substitute Ti<sup>4+</sup> into TiO<sub>2</sub> lattice, affecting light absorption characteristics of TiO<sub>2</sub> and charge separation between electrons and holes. The other is that the reduction of Fe<sup>3+</sup> ions to Fe<sup>2+</sup> ions by photoelectron on TiO<sub>2</sub> surface, inducing Fenton-like reaction for the enhancement of the ·OH formation rate in the plasma/TiO<sub>2</sub>/Fe<sup>3+</sup> system.

A detailed explanation will be discussed in section 3.2 and 3.3, respectively.

#### 3.2. Mechanisms of Fe<sup>3+</sup> ions for the enhancement of TiO<sub>2</sub> catalytic activity in visible light

To check whether the Fe<sup>3+</sup> decorated TiO<sub>2</sub> particles in pulsed discharge system, the characterization of TiO<sub>2</sub> structure was analyzed by XPS, UV-vis, and XRD. The sample of ITO1 was bare TiO<sub>2</sub> powder, and the samples of ITO2 and ITO3 were gained from plasma/TiO<sub>2</sub> and plasma/TiO<sub>2</sub>/Fe<sup>3+</sup> system with 60 min discharge treatment in distilled water, respectively.

The surface composition and chemical state of TiO<sub>2</sub> samples were firstly investigated by XPS analysis. Fig. 3(a) showed the fully scanned spectra of TiO<sub>2</sub> samples, where Ti, Fe, N, O and C elements appeared in ITO3 sample from plasma/TiO<sub>2</sub>/Fe<sup>3+</sup> system, while only Ti, O and C elements appeared in pure TiO<sub>2</sub> powder. Fig. 3(b) showed that the Ti 2p3/2 peak for ITO3 transferred to lower binding energy compared to that of pure TiO<sub>2</sub>, which might be due to the diffusion of Fe<sup>3+</sup> and nitrogen into TiO<sub>2</sub> lattice during plasma discharge process. Compared with normal XPS database, the binding energy at 709.9 eV was attributed to Fe<sub>2</sub>O<sub>3</sub> phase, and the binding energy at 711.5 eV was attributed to γ-FeOOH phase, as shown in Fig. 3(c). Similar results have reported previously [18,29], implying that the structure of Fe<sup>3+</sup> adsorbate on N-TiO<sub>2</sub> surfaces changed from Fe<sub>2</sub>O<sub>3</sub> to γ-FeOOH, and the generation of γ-FeOOH was responsible for the enhancement of photocatalytic activity in visible light. The Fe<sup>3+</sup> ion has stronger absorption on the TiO<sub>2</sub> surface through the Coulombic energy, due to its half-filled electronic configuration [30]. The pH of solution plays a significant role in controlling the structure of Fe<sup>3+</sup> adsorbate in a metal oxide or hydrolysable metal oxide. It has experimentally observed that the structure of Fe<sup>3+</sup> adsorbate on TiO<sub>2</sub> is hydrated metal oxides (forming [Fe (OH)]<sup>2+</sup>)

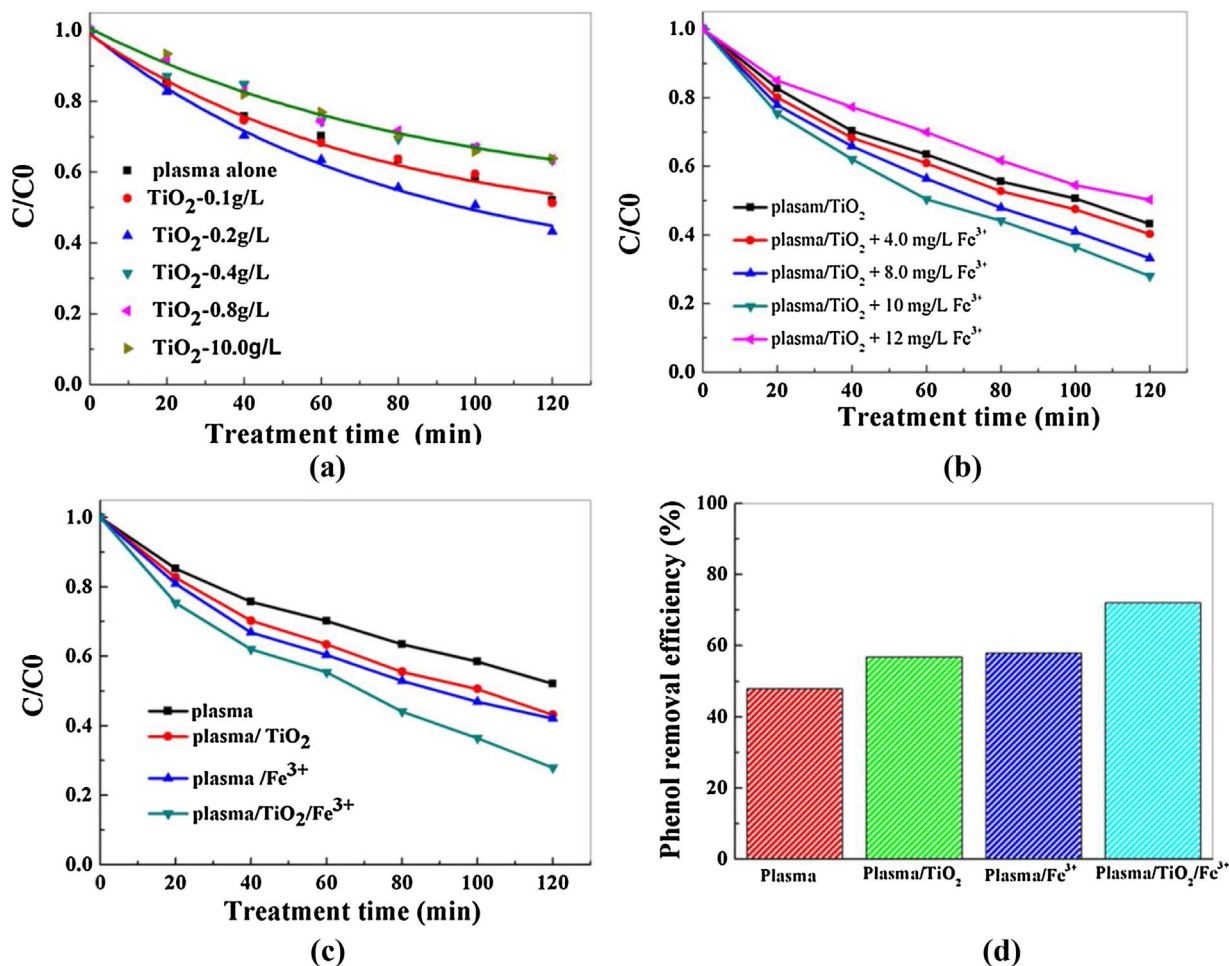


Fig. 2. (a) Effect of TiO<sub>2</sub> dosage on degradation of phenol by pulsed discharge; (b) Effect of Fe<sup>3+</sup> dosage on phenol degradation in plasma/TiO<sub>2</sub> system; (c) The changes of phenol concentration in plasma, plasma/TiO<sub>2</sub>, plasma/Fe<sup>3+</sup> and plasma/TiO<sub>2</sub>/Fe<sup>3+</sup>, respectively. (d) Phenol removal efficiency in plasma, plasma/TiO<sub>2</sub>, plasma/Fe<sup>3+</sup> and plasma/TiO<sub>2</sub>/Fe<sup>3+</sup>, respectively.

between pH 1.5 and 2.6 [31,32]. Fig. 4 showed that the pH of solution was below 3 after 20 min treatment due to generation of organic acids during phenol decomposition; hence the structure of Fe<sup>3+</sup> adsorbate on TiO<sub>2</sub> surfaces was mainly γ-FeOOH phase. After Fe<sup>3+</sup> ions were adsorbed on TiO<sub>2</sub> surfaces as γ-FeOOH phase, Fe<sup>3+</sup> from γ-FeOOH phase can quickly and easily substitute Ti<sup>4+</sup> into TiO<sub>2</sub> lattice because Fe<sup>3+</sup> and Ti<sup>4+</sup> have similar ionic radii (0.79 Å versus 0.75 Å) and γ-FeOOH phase is unstable on TiO<sub>2</sub> surface [33]. As a result, Fe<sup>3+</sup> ions have been successfully adsorbed on TiO<sub>2</sub> surface and then substituted Ti<sup>4+</sup> into titanium lattice, resulting in the Fe<sup>3+</sup> impurity level formed.

It is an interesting and noteworthy result that nitrogen element is clearly observed in ITO<sub>2</sub> and ITO<sub>3</sub>, while no peak assigned to nitrogen appeared in the spectrum of pure TiO<sub>2</sub> (ITO<sub>1</sub> sample). We can see that the Ti 2p<sub>3/2</sub> peak for ITO<sub>2</sub> sample from plasma/TiO<sub>2</sub> system also shift to lower binding energy, which may be due to the partial replacement of oxygen in the TiO<sub>2</sub> by nitrogen. As shown in Fig. 3(d), the peak at 396.2 eV was assigned to substitutional nitrogen in the structure of O-Ti-N; the peak at 400.1 eV was most likely due to N<sub>2</sub> in subsurface interstitial sites. This result indicated that oxygen atom in the O-Ti-O was substituted by nitrogen atom, leading to the formation of the Ti-N bonds in ITO<sub>2</sub> and ITO<sub>3</sub> sample. Air was used as bubbling gas in present study, whereas nearly 80% of the air was nitrogen. Nitrogen could be excited in discharge region to generate a high density of nitrogen atoms with high energy. Nitrogen element has been verified to be an effective doping element to modify the visible light absorption of TiO<sub>2</sub> because nitrogen atom has an atomic radius similar to the O atom [34]. In pulsed discharge process, therefore, the Ti-O bonds in TiO<sub>2</sub> could be

broken by nitrogen atoms with high energy, leading to N-Ti bond present in TiO<sub>2</sub>. Previous researches also indicated that N-doped TiO<sub>2</sub> could be prepared by plasma technology at a room temperature, in which the oxygen present in the TiO<sub>2</sub> was substituted by excited nitrogen with high energy [35,36]. The N-doped TiO<sub>2</sub> formed during plasma discharge process was also beneficial to enhance photocatalytic activity of TiO<sub>2</sub> in visible light. N-doped TiO<sub>2</sub> could successfully narrow the band gap of TiO<sub>2</sub> to absorb the visible light. More importantly, the co-doping with Fe<sup>3+</sup> and nitrogen led to much higher photocatalytic activity in visible light. The relative quantitative analysis of Fe and N element could be calculated by the XPS result using equation as follow equation [37,38].

$$n(E1)/n(E2) = [A(E1)/S(E2)]/[A(E2)/S(E2)] \quad (2)$$

where n was the number of the elemental atom, A was the XPS peak area, E was the element, and S was the elemental sensitivity factor. As a result, the molar ratio of Fe to N was 10: 1. Meanwhile, according the result of XPS, the nitrogen concentration was about 0.63 at.%, compared with oxygen concentration of 37.74 at.%. The x = 0.03 could be calculated from the structure formula of TiO<sub>2-x</sub>N<sub>x</sub>, which was consist with previous results where the value of x was usually lower than 0.04 [39,40].

To confirm whether the diffuse reflectance spectra of ITO<sub>2</sub> and ITO<sub>3</sub> increased the absorption in the visible region compared with pure TiO<sub>2</sub> (ITO<sub>1</sub>), the samples were characterized by UV-vis diffuse reflectance spectra. As shown in Fig. 5(a), the curve of ITO<sub>1</sub> sample (pure TiO<sub>2</sub>) showed absorption edge at around 400 nm, and only exhibited

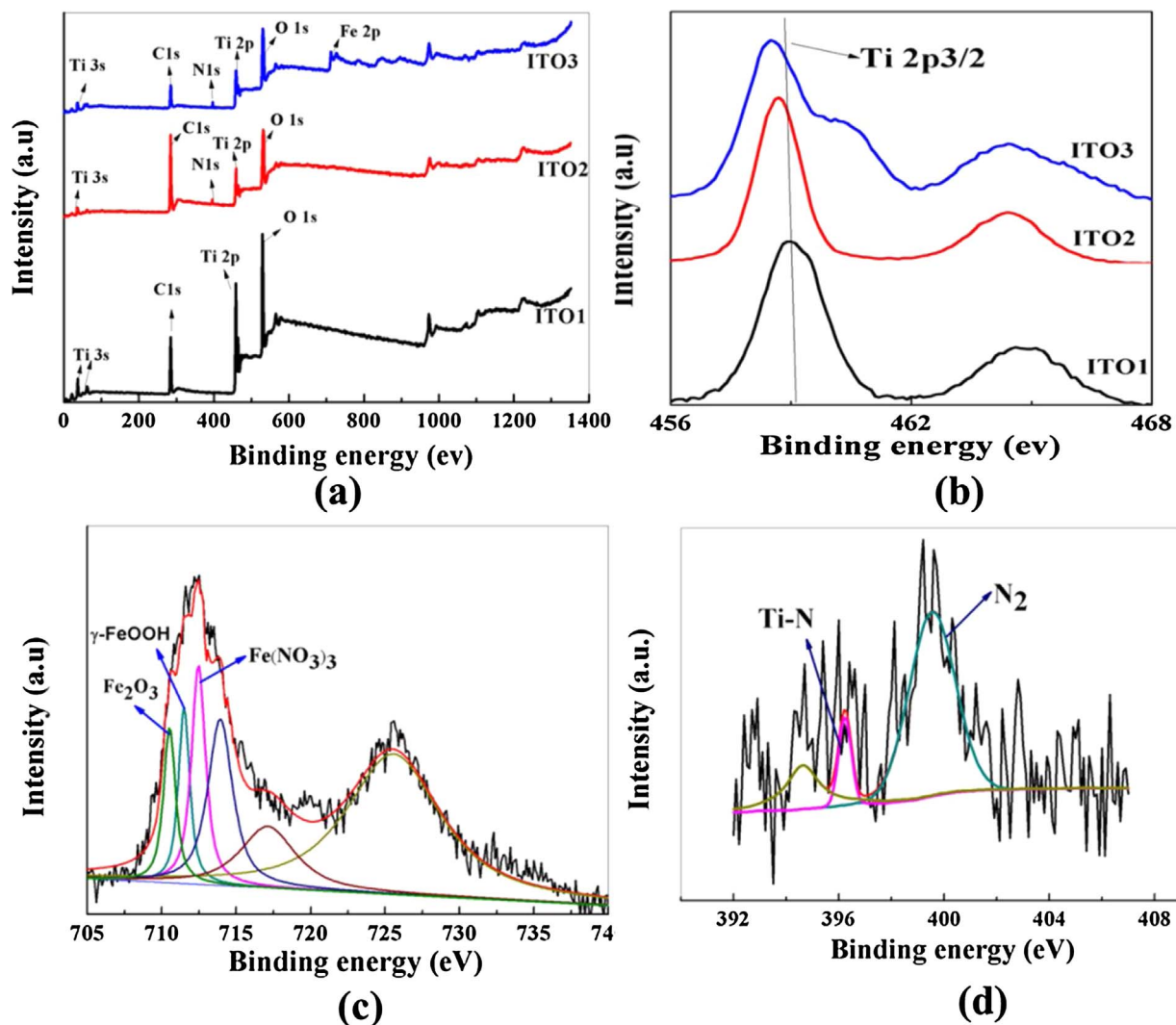


Fig. 3. (a) XPS fully scanned spectra of the  $\text{TiO}_2$ ; (b) XPS spectra of Ti 2p; (c) XPS spectrum of Fe 2p; (d) XPS spectra of N 1s (ITO1 from bare  $\text{TiO}_2$ -P25; ITO2 from plasma/ $\text{TiO}_2$  system; ITO3 from plasma/ $\text{TiO}_2/\text{Fe}^{3+}$  system).

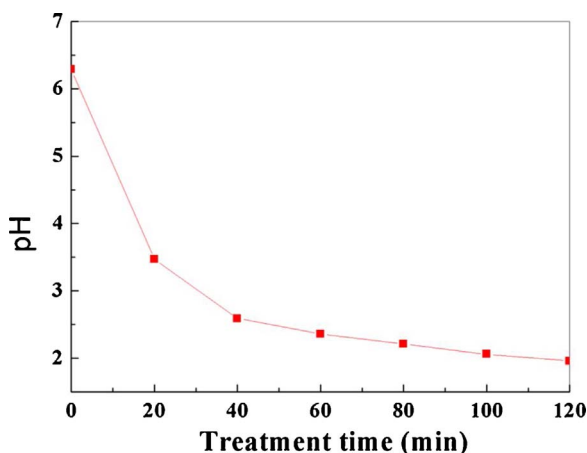


Fig. 4. The change of pH during the discharge process.

absorbance in the UV range. In contrast, the diffuse reflectance spectra of ITO2 and ITO3 samples have extended a red shifted and enhanced absorption in the visible light region. The results were consistent with XPS analysis. The spectrum of the ITO<sub>2</sub> sample showed an absorption edge at about 420 nm, which may be due to N-Ti bond present in  $\text{TiO}_2$ .

The spectrum of the ITO3 sample showed that a shoulder peak between 400 and 600 nm appeared, along with absorption in the UV region. The red shift of the absorption edge in ITO3 sample was attributed to the co-doping with  $\text{Fe}^{3+}$  and nitrogen on  $\text{TiO}_2$  inducing the band gap energy of  $\text{TiO}_2$  much narrower compared with the pure  $\text{TiO}_2$ . According to the Kubelka-Munk equations, the band gap energy of the ITO2 and ITO3 has been narrowed to 2.8 eV and 2.0 eV, respectively, as shown in Fig. 5(b).

After co-doping  $\text{Fe}^{3+}$  and nitrogen on  $\text{TiO}_2$  particle, nitrogen doping could form a new states just locating above the valence band for the substitutional nitrogen, and  $\text{Fe}^{3+}$  doping could produce the charge-transfer transition between the Fe 3d electron and  $\text{TiO}_2$  conduction band [29,41]. The electron exciting approaches have three possible pathways: from the valence band (VB) of  $\text{TiO}_2$  to the  $\text{Fe}^{3+}$  impurity level (pathway I), from the N impurity level to the  $\text{Fe}^{3+}$  impurity level (pathway II), from the N impurity level to the conduction band (CB) of  $\text{TiO}_2$  (pathway III), as shown in Scheme 1. These processes enhanced the yields of the photo-electrons and holes compared with the pure  $\text{TiO}_2$ , resulting in high photocatalytic activity. Furthermore, the co-doping with  $\text{Fe}^{3+}$  and nitrogen effectively inhibited the recombination rate of electron-hole pairs and prolonged their lifetime [42,43]. Fig. 6 showed the photocurrent responses (*I-t*) curve of the photoelectrodes consisting of ITO1, ITO2 and ITO3 samples. It was found that the stable photocurrent value of ITO2 and ITO3 samples was nearly 3 times and 5

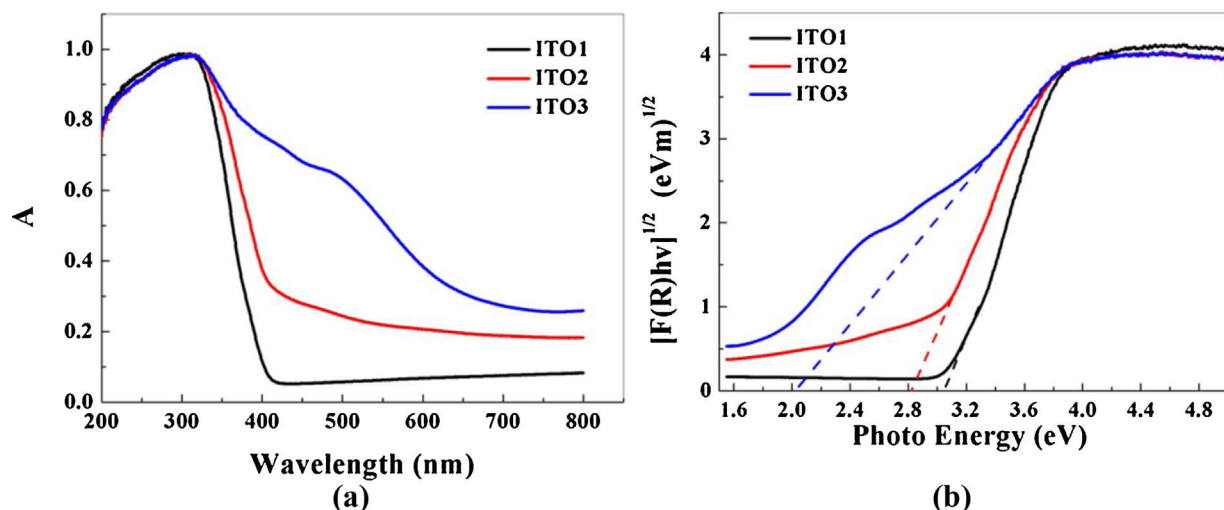
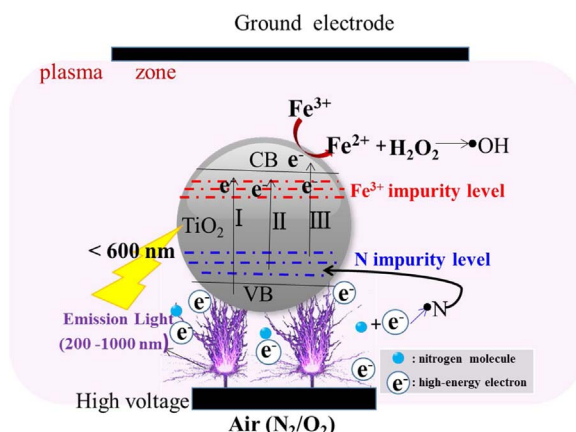


Fig. 5. (a) UV–vis spectra of different samples; (b)  $[F(R)hv]^{1/2}$  as a function of photo energy for different samples (ITO1 from bare  $TiO_2$ -P25; ITO2 from plasma/ $TiO_2$  system; ITO3 from plasma/ $TiO_2/Fe^{3+}$  system).



Scheme 1. The proposed mechanism of synergistic effect of  $Fe^{3+}$  and  $TiO_2$  in pulsed discharge plasma.

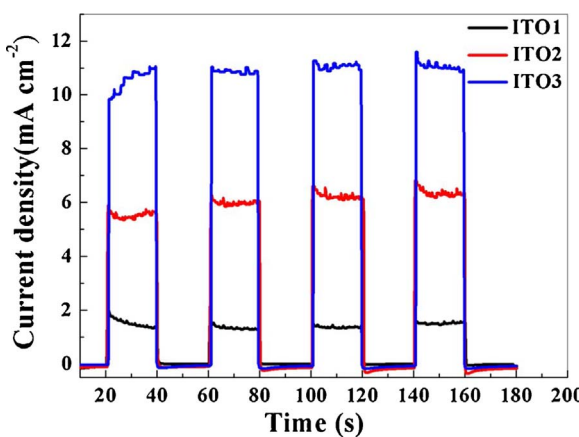


Fig. 6. The photocurrent responses of the film electrodes made of ITO1, ITO2 and ITO3 with a molar ratio of 1:10 M  $Na_2SO_4$  solution under visible-light irradiation. (ITO1 from bare  $TiO_2$ -P25; ITO2 from plasma/ $TiO_2$  system; ITO3 from plasma/ $TiO_2/Fe^{3+}$  system).

times higher than that of pure  $TiO_2$  (ITO1 sample), respectively. It could be ascribed to the doped  $Fe^{3+}$  and nitrogen that improved the separation rate of photo-generated electrons and holes, and resulting in enhanced photocurrent. On the one hand, the doped nitrogen can enhance the trapping rate of photo-generated charge carriers due to an increase in oxygen vacancies [44,45]. On the other hand,  $Fe^{3+}$  can

inhibit the recombination of electrons and holes due to the reason that  $Fe^{3+}$  is effective electrons and holes trap without causing a significant crystalline distortion. The  $Fe^{2+}$  species can be formed by means of photoelectron transfer from valence band (VB) and/or N impurity level to  $Fe^{3+}$  to form  $Fe^{2+}/Fe^{3+}$  energy level. The photoelectron in  $Fe^{2+}$  can be easily transferred to a neighboring surface  $Ti^{4+}$  because the  $Fe^{2+}/Fe^{3+}$  energy level lies close to  $Ti^{3+}/Ti^{4+}$  level, which then leads to interfacial electron transfer [46], according to the reactions (3–5).  $Fe^{3+}$  can also serve as hole trap due to the energy level for  $Fe^{3+}/Fe^{4+}$  above the valence band (VB) of  $TiO_2$  (reaction 6). It should be noteworthy, however, that  $Fe^{3+}$  ions may act as recombination centers at higher  $Fe^{3+}$  doped amount (reaction 7–8).



Fig. 7 illustrated the XRD patterns of the ITO1, ITO2, and ITO3 samples.

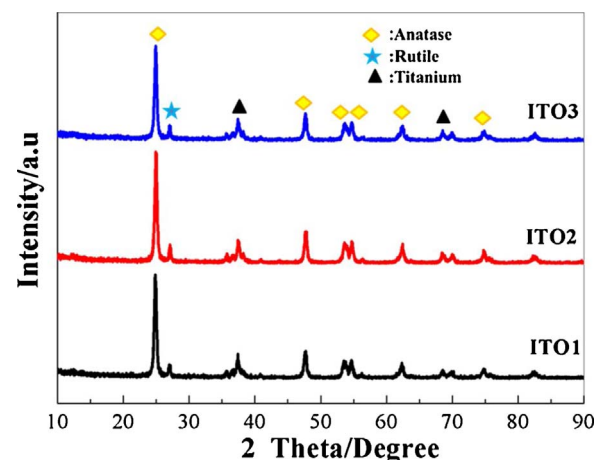


Fig. 7. XRD patterns of the  $TiO_2$  samples. (ITO1 from bare  $TiO_2$ -P25; ITO2 from plasma/ $TiO_2$  system; ITO3 from plasma/ $TiO_2/Fe^{3+}$  system).

Table 1

Data of diffraction peaks obtained from XRD patterns of  $\text{TiO}_2$  (101) samples. (ITO1 from bare  $\text{TiO}_2$ -P25; ITO2 from plasma/ $\text{TiO}_2$  system; ITO3 from plasma/ $\text{TiO}_2/\text{Fe}^{3+}$  system).

Sample	2θ (deg.)	Peak area <sup>a</sup> (counts deg.)	Full width at half maximum (deg.)	Crystallite size (nm)
ITO1	24.821	10396	0.443	18.9
ITO2	24.979	11096	0.434	19.3
ITO3	24.920	9301	0.425	19.7

All samples contained major anatase phase and trace rutile phase. The results indicated that the bulk structure of the  $\text{TiO}_2$  particle was not changed after the plasma discharge treatment. It was noteworthy that no iron oxide ( $\gamma\text{FeOOH}$  17.98°) or Ti-N phase appeared in the XRD spectra. As acknowledged in some of these papers [20,27,47], XRD may not detect Fe and N dopant substitution because the amount of formed phase is below the detection limit of XRD or the Fe and nitrogen is highly dispersed on the  $\text{TiO}_2$  surface.

Meanwhile, the crystallite size of all  $\text{TiO}_2$  samples was calculated using the Debye-Scherrer equation on the anatase (101) and the values were given in Table 1. The crystallite size of the ITO3 sample from plasma/ $\text{TiO}_2/\text{Fe}^{3+}$  system was higher than that of the bare  $\text{TiO}_2$  and the ITO1 sample from plasma/ $\text{TiO}_2$  system, in which Fe and nitrogen doping was beneficial to growth of crystal. Similar results have been drawn in previously researches [27,48]. The crystallite size has recognized as an important factor for photocatalytic activity. The crystallite size mainly alters the electronic properties of anatase and therefore affects the recombination rate of photo-generated electrons and holes. It has been reported that the photo-activity was found to increase with increasing crystallite size because the recombination rate of electron-hole pairs was slower [49,50]. Therefore, the separation rate of photo-electrons and holes increased due to the co-doping of  $\text{Fe}^{3+}$  and nitrogen, which are consistent with results of photocurrent analysis.

Furthermore, the co-doping of the  $\text{Fe}^{3+}$  ions and nitrogen greatly enhanced the utilization efficiency of plasma energy due to high photocatalytic activity in the visible light region (400 ~ 600 nm). Fig. 8 showed typical optical emission spectrum observed from the underwater pulsed discharge. For the visible light wavelength range (400–600 nm) was observed under air atmosphere, this spectrum was dominated by the nitrogen lines from  $\text{N}_2$  ( $\text{C}^3\pi_u\text{-B}^3\pi_g$ ), which could be effectively utilized by the nitrogen and  $\text{Fe}^{3+}$  co-doped  $\text{TiO}_2$  to produce more  $\cdot\text{OH}$ .

### 3.3. Increase $\cdot\text{OH}$ concentration by inducing fenton-like reaction

It is well known that irradiation of the  $\text{TiO}_2$  with high energy input induces the generation of excited-state conduction band electrons ( $e^-$ )

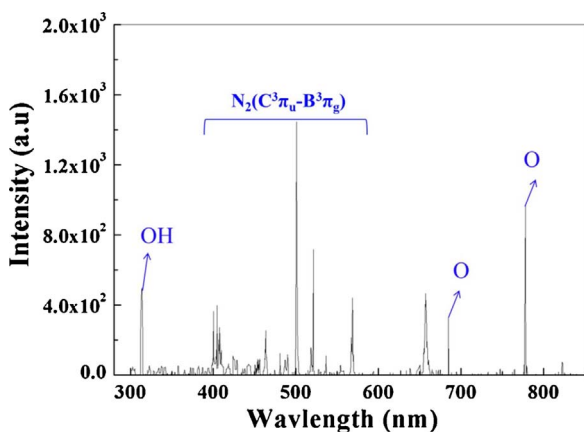
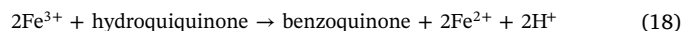
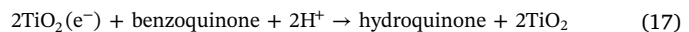
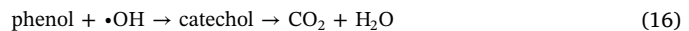
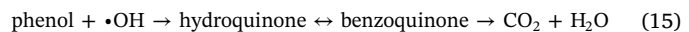
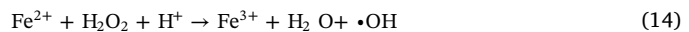
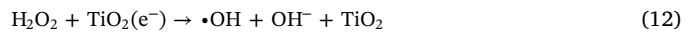
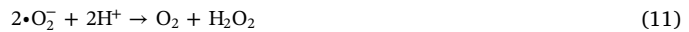


Fig. 8. Optical emission spectrum from pulsed discharge in air gas atmospheres.

and valence band holes ( $h^+$ ) pairs. The electrons could be react with  $\text{O}_2$  to generate upper oxide radical anion ( $\text{O}_2^{\bullet-}$ ), which will further react with  $\text{H}_2\text{O}$  to form  $\cdot\text{OH}$ . The holes will also oxidize either  $\text{H}_2\text{O}$  molecule or  $\text{OH}^-$  anions to form  $\cdot\text{OH}$ . These processes are described by Eqs 9–12. However, it has proved that the transfer of electrons from  $\text{TiO}_2$  ( $e^-$ ) to  $\text{O}_2$  was blocked by  $\text{Fe}^{3+}$ , because of highly adsorptive capacity of  $\text{TiO}_2$  to  $\text{Fe}^{3+}$  ions, and more positive potential of  $\text{Fe}^{3+}/\text{Fe}^{2+}$  (0.771 V) than the conduction band of  $\text{TiO}_2$  (-0.5 V) [15]. We believe that  $\text{Fe}^{3+}$  ions not only play a role in co-doping with nitrogen which leaded to high photocatalytic activity in visible light region, but also involve in electron-transfer process in plasma/ $\text{TiO}_2/\text{Fe}^{3+}$  system.

To demonstrate the role of  $\text{Fe}^{3+}$  in electron-transfer pathway, we followed the evolution of  $\text{Fe}^{2+}$  and total irons concentration during phenol degradation in plasma/ $\text{Fe}^{3+}$  system and in plasma/ $\text{TiO}_2/\text{Fe}^{3+}$  system, and as control experiments, the  $\text{Fe}^{2+}$  and total irons concentration were also analyzed in distilled water. As shown in Fig. 9(a), the concentration of  $\text{Fe}^{2+}$  ions in the discharge with  $\text{TiO}_2$  was higher than that without  $\text{TiO}_2$ . For example, only 0.8 mg  $\text{L}^{-1}$  of  $\text{Fe}^{2+}$  was generated during 60 min of discharge treatment without  $\text{TiO}_2$  in phenol solution, while it increased to 1.2 mg  $\text{L}^{-1}$  with  $\text{TiO}_2$  in phenol solution. Similar trends were also presented in distilled water. This might be attributed to the reduction of  $\text{Fe}^{3+}$  to  $\text{Fe}^{2+}$  using photo-electrons on  $\text{TiO}_2$  (reaction 13). Moreover, the total irons concentration in solution was determined with or without  $\text{TiO}_2$ , as shown Fig. 9(b). It could be seen that the introduction of  $\text{TiO}_2$  significantly decreased total irons concentration in solution. For example, the total irons concentration was 7.6 mg  $\text{L}^{-1}$  after 60 min of discharge treatment in plasma/ $\text{Fe}^{3+}$  system, which was only 4.6 mg  $\text{L}^{-1}$  in plasma/ $\text{Fe}^{3+}/\text{TiO}_2$  system. This was probably because  $\text{Fe}^{3+}$  ions doped on  $\text{TiO}_2$  particles, and hence  $\text{Fe}^{3+}$  ions lost from discharge solution.



It was important to note that the concentration of  $\text{Fe}^{2+}$  ions generated in discharge processes with phenol was higher than that generated in the discharge process without phenol. This was due to the intermediates of hydroquinone for the reductive reaction of  $\text{Fe}^{3+}$  (reaction 18). We followed the evolution of hydroquinone and benzoquinone concentration during the phenol decomposition process, as demonstrated in Fig. 10(a–b). It could be seen that the accumulation of hydroquinone was observed in plasma/ $\text{TiO}_2$  system after 40 min, whereas the benzoquinone amounts decreased with an addition of  $\text{TiO}_2$ . The hydroquinone concentration reached a maximum of 7 mg  $\text{L}^{-1}$  with addition of  $\text{TiO}_2$ , which nearly 2 times greater than those in plasma alone system. Similar observations have also been reported previously [51,52], where *p*-benzoquinone reduction was selectively catalyzed on  $\text{TiO}_2$  surfaces, implying that the hydroquinone pathway was the limiting step for phenol degradation in the presence of  $\text{TiO}_2$ .

In pulsed plasma discharge system, phenol can undergo a ring cleavage by the nonselective attack of  $\cdot\text{OH}$ , where the hydroxylated phenolic by-product mainly hydroquinone, benzoquinone and catechol are generated (reaction 15–16). Benzoquinone produced from phenol

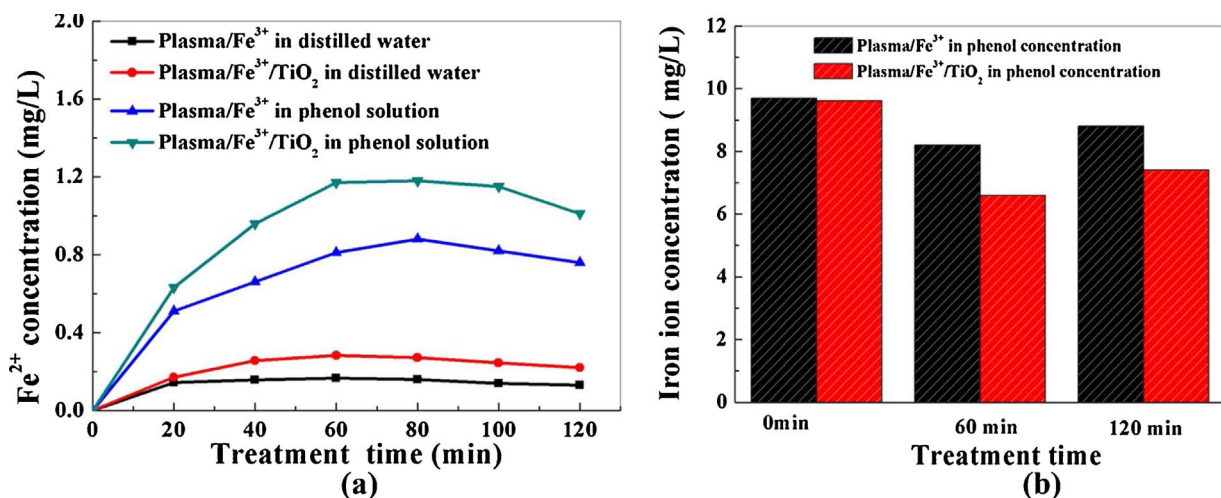


Fig. 9. (a) The changes of  $\text{Fe}^{2+}$  concentration in plasma/ $\text{Fe}^{3+}$  in distilled water, plasma/ $\text{TiO}_2/\text{Fe}^{3+}$  in distilled water, plasma/ $\text{Fe}^{3+}$  in phenol solution and plasma/ $\text{TiO}_2/\text{Fe}^{3+}$  in phenol solution, respectively. (b) The total iron ions concentration in plasma/ $\text{Fe}^{3+}$  in phenol solution and plasma/ $\text{TiO}_2/\text{Fe}^{3+}$  in phenol solution, respectively.

may be reduced to hydroquinone using the electrons on  $\text{TiO}_2$  surface (reaction 17), which results in the observed accumulation of hydroquinone. This redox reaction significantly inhibits the overall phenol decomposition because free photo-electrons on  $\text{TiO}_2$  surface rapidly consumes in an ineffective manner, where photo-electrons cannot ultimately generate to  $\cdot\text{OH}$ . As  $\text{Fe}^{3+}$  ions were supplied to plasma/ $\text{TiO}_2$ , the photo-electrons would have a greater probability to react with  $\text{Fe}^{3+}$  ions, rather than with *p*-benzoquinone. This lead to the successful progress of plasma induced Fenton-like reaction (reaction 14) for the enhancement of the degradation of phenol under high  $\text{Fe}^{2+}$  concentration in the plasma/ $\text{TiO}_2/\text{Fe}^{3+}$  system. This conclusion could also be confirmed by the concentration of  $\cdot\text{OH}$  which increased from  $14.8 \times 10^{-5} \text{ mol L}^{-1}$  in the plasma/ $\text{TiO}_2$  system to  $20.6 \times 10^{-5} \text{ mol L}^{-1}$  in the plasma/ $\text{TiO}_2/\text{Fe}^{3+}$  system, as shown in Fig. 11.

On the basis of the above results, the synergistic effect of  $\text{Fe}^{3+}$  and  $\text{TiO}_2$  in pulsed discharge occurs because: (1) The co-doped of  $\text{Fe}^{3+}$  and nitrogen on  $\text{TiO}_2$  particles leads to more narrow band gap of  $\text{TiO}_2$  (2.0 eV) and increases the separation rate of photo-generated electrons and holes, therefore enhances the photo-reactivity in visible light (< 600 nm), which improves the utilization efficiency of plasma energy. (2) Photoelectrons voluntarily participated in the reduction from  $\text{Fe}^{3+}$  to  $\text{Fe}^{2+}$  on  $\text{TiO}_2$  particles surface, inducing Fenton-like reaction for the enhancement of the  $\cdot\text{OH}$  production, which also can be

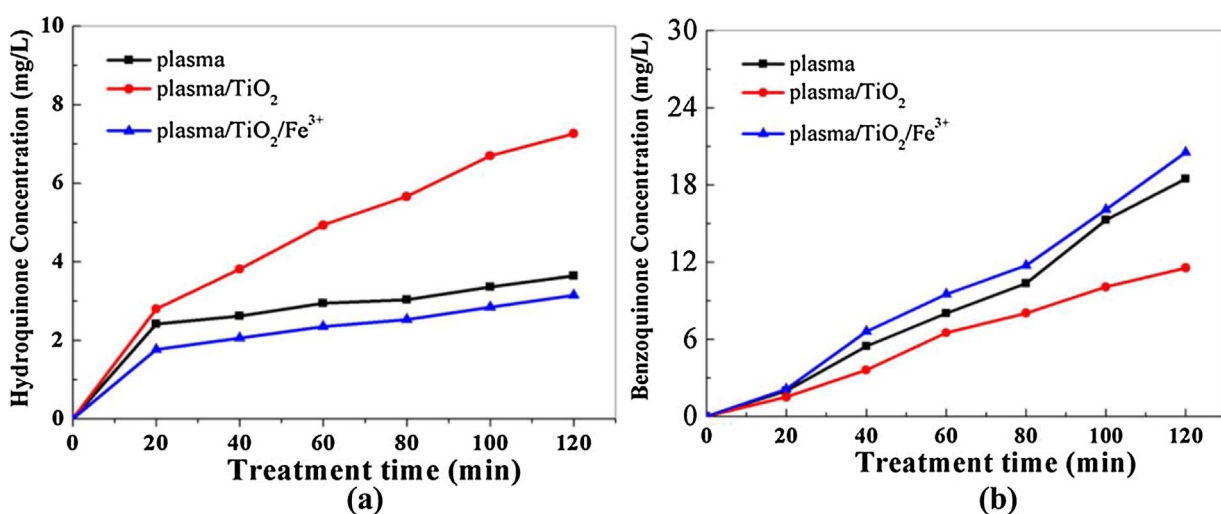


Fig. 10. (a) The changes of hydroquinone concentration; (b) The changes of benzoquinone concentration.

probe molecule under air atmosphere. Our results suggested that  $\text{Fe}^{3+}$  not only played a role in co-doping with nitrogen which enhanced  $\text{TiO}_2$  photocatalytic activity under visible light, but also involved in electron-transfer process in plasma/ $\text{TiO}_2/\text{Fe}^{3+}$  system. XPS analysis of  $\text{TiO}_2$  from plasma/ $\text{TiO}_2/\text{Fe}^{3+}$  system showed that the  $\text{Fe}^{3+}$  ions and nitrogen successful doped on  $\text{TiO}_2$  particles. The UV-vis spectrum indicated that the co-doping of the  $\text{Fe}^{3+}$  ions and nitrogen narrowed the band gap of  $\text{TiO}_2$  to 2.0 eV and greatly enlarged the absorption edge at around 600 nm. The photocurrent analysis illustrated that the  $\text{Fe}^{3+}$  and nitrogen doped on  $\text{TiO}_2$  effectively inhibited the recombination rate of photo-generated electrons and holes. In plasma/ $\text{TiO}_2$  system, the reduction of benzoquinone to hydroquinone consumed photo-electrons in an ineffective manner, thus suppressing phenol decomposition. As  $\text{Fe}^{3+}$  ion were supplied to plasma/ $\text{TiO}_2$  system, the photo-electrons reacted with  $\text{Fe}^{3+}$  ion, rather than with *p*-benzoquinone. The regeneration of  $\text{Fe}^{3+}$  to  $\text{Fe}^{2+}$  by photo-electrons reduction lead to the successful progress of plasma induced Fenton-like reaction for the enhancement of the degradation of phenol in the plasma/ $\text{TiO}_2/\text{Fe}^{3+}$  system.

## Acknowledgments

The authors thank the Projects funded by the Fundamental Research Funds for the Central Universities under Grant (DUT 15QY17) and the National Natural Science Foundation, P. R. China (Project No.51477025 and NO. U1462105) for their financial support to this research.

## References

- [1] B. Jiang, J. Zheng, S. Qiu, M. Wu, Q. Zhang, Z. Yan, Q. Xue, *Chem. Eng. J.* 236 (2014) 348–368.
- [2] F.L. Fu, D.D. Dionysiou, H. Liu, *J. Hazard Mater.* 267 (2014) 194–205.
- [3] M.A. Oturan, J.J. Aaron Crit, *Rev. Environ. Sci. Technol.* 44 (23) (2014) 2577–2641.
- [4] B.R. Locke, M. Sato, P. Sunka, M.R. Hoffmann, J.-S. Chang, *Ind. Eng. Chem. Res.* 45 (2006) 882–905.
- [5] P. Šunka, *Phys. Plasmas.* 8 (5) (2001) 2587–2594.
- [6] B. Sun, M. Sato, J.S. Clements, *Environ. Sci. Technol.* 34 (2000) 509–513.
- [7] A. Abou-Ghazala, S. Katsuki, K.H. Schoenbach, F.C. Dobbs, K.R. Moreira, *IEEE Trans. Plasma Sci.* 30 (2004) 1449–1453.
- [8] M.A. Malik, A. Ghaffar, S.A. Malik, *Plasma. Sources. Sci. Technol.* 10. 1 (2001) 82–91.
- [9] T.C. Wang, N. Lu, J. Li, Y. Wu, *Environ. Sci. Technol.* 45 (2011) 9301–9307.
- [10] X.L. Hao, M.H. Zhou, L.C. Lei, *J. Hazard Mater.* 141 (2007) 475–482.
- [11] Y. Zhang, J. Liu, X. Wang, X. Qing, Y. Cong, Q. Wang, C. Li, *J. Colloid. Interface. Sci.* 44 (2013) 104–111.
- [12] M.R. Ghezzar, F. Abdelmalek, M. Belhadj, N. Benderdouche, A. Addou, *Appl. Catal. B: Environ.* 72 (2007) 304–313.
- [13] H.J. Wang, J. Li, X. Quan, Y. Wu, *Appl. Catal. B: Environ.* 83 (2008) 72–77.
- [14] P. Lukes, M. Clupek, V. Babicky, P. Sunka, *Plasma. Sources. Sci. Technol.* 17 (2008) 024012 (11pp).
- [15] J.Y. Wang, Z.H. Liu, B.X. Cai, *Environ. Sci. Technol.* 42 (2008) 5759–5764.
- [16] G.R. Bamwenda, T. Uesugi, Y. Abe, K. Sayama, H. Arakawa, *Appl. Catal. A.* 205 (2001) 117–128.
- [17] T. Aarthi, G. Madras, *Ind. Eng. Chem. Res.* 46 (2007) 7–14.
- [18] M.Y. Xing, J.L. Zhang, F. Chen, *J. Phys. Chem. C.* 113 (2009) 12848–12853.
- [19] M.S. Nahar, K. Hasegawa, S. Kagaya, *Chemosphere* 65 (2006) 1976–1982.
- [20] M.H. Zhou, J.G. Yu, B. Cheng, *J. Hazard. Mater.* 137 (3) (2006) 1838–1847.
- [21] M. Liu, X. Qiu, M. Miyachi, K. Hashimoto, *J. Am. Chem. Soc.* 135 (27) (2013) 10064–10072.
- [22] X.L. Hao, M.H. Zhou, Q. Xin, L.C. Lei, *Chemosphere* 66 (2007) 2185–2192.
- [23] L. Diez, M.-H. Livertoux, A.-A. Stark, M. Wellman-Rousseau, P. Leroy, *J. Chromatogr. B.* 763 (2001) 185–193.
- [24] P. Teismann, B. Ferger, *Brain Res. Protocols.* 5 (2000) 204–210.
- [25] P. Lukes, M. Clupek, P. Sunka, F. Peterka, T. Sano, N. Negishi, S. Matsuzawa, K. Takeuchi, *Res. Chem. Intermed.* 31 (2005) 285–294.
- [26] I.K. Konstantinou, T.A. Albanis, *Appl. Catal. B: Environ.* 49 (2004) 1–14.
- [27] H.Y. Hao, J.L. Zhang, *Microporous. Mesoporous. Mater.* 121 (2009) 52–57.
- [28] S. George, S. Pokhrel, Z.X. Ji, B.L. Henderson, X.L.J. Tian, Li, J.I. Zink, A.E. Nel, L. Mäder, *J. Am. Chem. Soc.* 133 (29) (2011) 11270–11278.
- [29] J. Yu, Q. Xiang, M. Zhou, *Appl. Catal. B: Environ.* 90 (2009) 595–602.
- [30] A.N. Mangham, N. Govind, M.E.V. Bowden, Shutthanandan, A.G. Joly, M.A. Henderson, S.A. Chambers, *J. Phys. Chem. C* 115 (2011) 15416–15424.
- [31] E. Piera, M.I. Tejedor-Tejedor, M.E. Zorn, M.A. Anderson, *Appl. Catal. B: Environ.* 46 (2003) 671–685.
- [32] R.H. Byrne, Y.R. Luo, R.W. Young, *Mar. Chem.* 70 (1) (2000) 23–35.
- [33] J. Zhu, W. Zheng, B. He, J. Zhang, M. Anpo, *J. Mol. Catal. A: Chem.* 216 (2004) 35–43.
- [34] R. Asahi, T. Morikawa, T. Ohwaki, K. Aoki, T. Taga, *Science* 293 (2001) 269–271.
- [35] K. Matsubara, M. Danno, M. Inoue, Y. Honda, T. Abe, *Chem. Eng. J.* 181–182 (2012) 754–760.
- [36] L. Han, Y. Xin, H. Liu, X. Ma, G. Tang, *J. Hazard. Mater.* 175 (2010) 524–531.
- [37] J. Mu, B. Chen, M. Zhang, Z. Guo, P. Zhang, Z. Zhang, Y. Sun, C. Shao, Y. Liu, *ACS Appl. Mater. Interfaces.* 4 (2012) 424–430.
- [38] J.H. Li, D.Z. Shen, J.Y. Zhang, D.X. Zhao, B.S. Li, Y.M. Lu, Y.C. Liu, X.W. Fan, *J. Magn. Magn. Mater.* 302 (2006) 118–121.
- [39] H. Irie, Y. Watanabe, K. Hashimoto, *J. Phys. Chem. B* 107 (23) (2003) 5483–5486.
- [40] H. Li, J. Li, Y. Huo, *J. Phys. Chem. B* 110 (4) (2006) 1559–1565.
- [41] Y. Cong, J.L. Zhang, F. Chen, M. Anpo, D. He, *J. Phys. Chem. C* 111 (2007) 10618–10623.
- [42] T. Tong, J. Zhang, B. Tian, F. Chen, D. He, *J. Hazard. Mater.* 155 (2008) 572–579.
- [43] X. Shen, J. Guo, Z. Liu, S. Xie, *Appl. Surface. Sci.* 254 (2008) 4726–4731.
- [44] R. Asahi, T. Morikawa, H. Irie, T. Ohwaki, *Chem. Rev.* 114 (19) (2014) 9824–9852.
- [45] T. Ihara, M. Miyoshi, M. Ando, S. Sugihara, Y. Iriyama, *J. Mater. Sci.* 36 (2001) 4201–4207.
- [46] Z. Ambros, N. Balázs, T. Alapi, G. Wittmann, P. Sipos, A. Dombi, K. Mogyorósi, *Appl. Catal. B: Environ.* 81 (2008) 27–37.
- [47] C.Y. Wang, C. Böttcher, D.W. Bahnemann, J.K. Dohrmann, *J. Mater. Chem.* 13. 9 (2003) 2322–2329.
- [48] C. Adán, A. Bahamonde, M. Fernández-García, A. Martínez-Arias, *Appl. Catal. B* 72 (1) (2007) 11–17.
- [49] X.Q. Wang, L. Sø, R. Su, S. Wendt, P. Hald, A. Mamakhe, C.X. Yang, Y.D. Huang, B.B. Lversen, F. Besenbacher, *J. Catal.* 310 (2014) 100–108.
- [50] C.B. Almquist, P. Biswas, *J. Catal.* 212 (2002) 145–156.
- [51] R. Su, R. Tirucalam, Q. He, N. Dimitratos, L. Kesavan, C. Hammond, J.A. Lopez-Sánchez, R. Bechstein, C.J. Kiely, G.J. Hutching, F. Besenbacher, *ACS. Nano* 7 (2012) 6284–6292.
- [52] K. Nagaveni, G. Sivalingam, M.S. Hegde, G. Madras, *Environ. Sci. Technol.* 38 (2004) 1600–1604.